SANDIA REPORT
SAND2021-11278
Printed September 2021

Sandia National Laboratories

Rock Valley Accelerated Weight Drop Seismic Data Processing and Picking of P-wave and S-wave Arrival Times

Jennifer L. Harding, Miles Bodmer, Leiph Preston

Prepared by
Sandia National Laboratories
Albuquerque, New Mexico
87185 and Livermore,
California 94550

Issued by Sandia National Laboratories, operated for the United States Department of Energy by National Technology & Engineering Solutions of Sandia, LLC.

Available to DOE and DOE contractors from
U.S. Department of Energy
Office of Scientific and Technical Information
P.O. Box 62
Oak Ridge, TN 37831

Telephone: (865) 576-8401
Facsimile: (865) 576-5728
E-Mail: reports@osti.gov
Online ordering: http://www.osti.gov/scitech

Available to the public from
U.S. Department of Commerce
National Technical Information Service
5301 Shawnee Rd
Alexandria, VA 22312

Telephone: (800) 553-6847
Facsimile: (703) 605-6900
E-Mail: orders@ntis.gov
Online order: https://classic.ntis.gov/help/order-methods/

ABSTRACT

Rock Valley, in the southern end of the Nevada National Security Site, hosts a fault system that was responsible for a shallow (< 3 km below surface) magnitude 3.7 earthquake in May 1993. In order to better understand this system, seismic properties of the shallow subsurface need to be better constrained. In April and May of 2021, accelerated weight drop (AWD) active-source seismic data were recorded in order to measure P- and S-wave travel-times for the area. This report describes the processing and phase picking of the recorded seismic waveforms. In total, we picked 7,982 P-wave arrivals at offsets up to ~2500 m, and 4,369 S-wave arrivals at offsets up to ~2200 m. These travel-time picks can be inverted for shallow P-wave and S-wave velocity structure in future studies.

ACKNOWLEDGEMENTS

This work was made possible by the National Nuclear Security Administration (NNSA), Defense Nuclear Nonproliferation Research and Development (DNN R&D), and everyone involved with the Source Physics Experiment (SPE). The authors would also like to thank Robert White, Reagan Turley, and Cleat Zealer for their efforts in the field, as well as Rob Abbott for his input on analysis.

This paper describes objective technical results and analysis. Any subjective views or opinions that might be expressed in the paper do not necessarily represent the views of the U.S. Department of Energy or the United States Government.

CONTENTS

LIST OF FIGURES

LIST OF TABLES

This page left blank

ACRONYMS AND DEFINITIONS

Abbreviation	Definition
AWD	Accelerated Weight Drop
CMSL	CREWES MATLAB Software Library
CREWES	Consortium for Research in Elastic Wave Exploration Seismology
EW	East-West
GPS	Global Positioning System
ms	millisecond
NNSS	Nevada National Security Site
NS	North-South
NTS	Nevada Test Site
P-wave	Compressional wave
RV	Rock Valley
RVDC	Rock Valley Direct Comparison
RVFZ	Rock Valley Fault Zone
sps	Samples per second
S-wave	Shear wave
UTM	Universal Transverse Mercator

This page left blank

1. INTRODUCTION

A cluster of shallow (<3 km depth below surface) earthquakes occurred in Rock Valley (RV) along the Rock Valley Fault Zone (RVFZ), southern Nevada National Security Site (NNSS) in May of 1993 (Smith et al., 2000). In order to better constrain properties of the shallow subsurface, thereby improving the locations of these earthquakes and faults within the RVFZ, accelerated weight drop (AWD) active-source seismic data were collected in April and May of 2021 as a part of the Rock Valley Direct Comparison (RVDC) Experiment. This report details the collection, processing, and P-wave (compressional wave) and S-wave (shear wave) arrival time picking of the AWD data to produce P-wave and S-wave travel-time datasets. The travel-time data sets are available to program researchers and can be obtained via correspondence with the authors. A preliminary P-wave tomography study using this dataset can be found in Preston & Harding (2021).

This page left blank

2. ROCK VALLEY OVERVIEW

Rock Valley (RV) sits at the southern edge of the Nevada National Security Site (NNSS), formerly known as the Nevada Test Site (NTS)(Figure 2-1a). The northeast-trending valley is bounded by Skull Mountain to the north, the Specter Range to the south, Little Skull Mountain to the northwest, Jackass Flat to the west, Frenchman Flat to the east, and Red Mountain to the southeast (Figure 2-1a). The Rock Valley Fault Zone (RVFZ) is an approximately 4-km-wide zone of northeast-trending faults and other structures associated with faulting within RV (Figure 2-1b). The termini of the fault zone have not been mapped, as the RVFZ is covered in the west and east by the alluvium of Jackass and Frenchman Flats, respectively, leading to an estimated length ranging from 20 to 40 km (O'Leary, 2000). RV separates Miocene volcanic rocks of Little Skull and Skull Mountains to the north from older, Upper-Cambrian to Ordovician carbonates in the southern mountain ranges (O'Leary, 2000; Slate et al., 1999)(Figure 2-1c). RV itself hosts mostly Quaternary alluvial deposits and Miocene sedimentary rocks (O'Leary, 2000; Slate et al., 1999) (Figure 2-1c). See Figure 2-1c for geologic mapped units in the RV region, after Slate et al. (1999), wherein detailed unit descriptions can be found. Appendix A summarizes the correlation of all NNSS mapped units (Slate et al., 1999).

The main faults in the RVFZ are left-lateral strike-slip, and have been mapped and collated (Slate et al., 1999, Yount et al., 1987)(Figure 2-1b, Figure 2-1c, Figure 3-1). The estimated lifetime-averaged slip rate of the RVFZ is 0.089 mm/yr, beginning ~30 Ma (Barnes et al., 1982, O'Leary, 2000, Kane & Brecken, 1983). In May 1993, a magnitude 3.7 earthquake occurred in the RVFZ, the largest ever recorded in the fault zone, at a depth < 3km (Pyle et al., 2015; Smith et al., 2000). This earthquake triggered over 600 events over the next 5 months, and other magnitude >3.5 events have been recorded on regional seismic networks through 1998 (Smith et al., 2000). It is possible that these earthquakes were triggered by a magnitude 5.6 event at Little Skull Mountain in 1992, after which seismic activity in the RVFZ increased (Smith et al., 2000).

Previous seismic studies within or surrounding RV include 1-D seismic reflection profiles (Majer et al. 1996), and regional seismic velocity models (Preston et al. 2007; Preston et al., 2019), which image relatively low (<5 km/s) P-wave velocities and a Vp/Vs ratio of ~1.65 at ~2 km depth blow surface along RV.

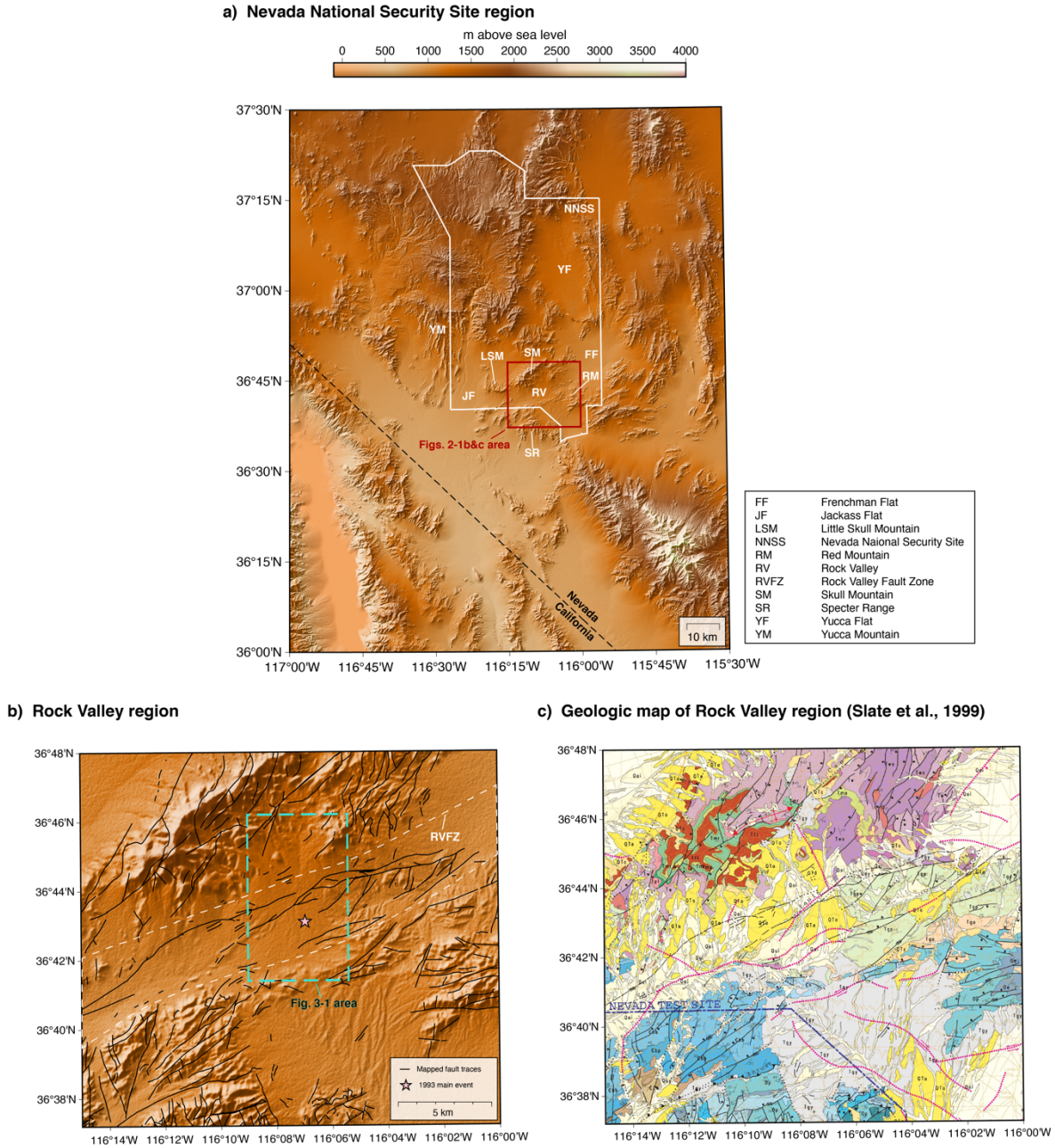

Figure 2-1. Regional maps of the Nevada National Security Site and Rock Valley

3. AWD DATA

3.1. Data Collection

The RVDC seismic array consists of 188 seismometers deployed at ~100 m spacing on several linear transects (see Figure 3-1). The main deployment follows two roads which intersect to form an inverted "Y". Several short lines connect the roads in the southern section and an extended line continues off to the northwest, following a rough projection of the northwest-southeast trending road. The sensors used were 3 component DT-SOLO 5 Hz geophones connected to a Hawk Field Station Unit (INOVA) datalogger. Seismic data were collected at a sampling rate of 500 samples per second (sps) and with instruments recording continuously throughout the duration of the active source experiment. Health of the array was monitored in real time during the active source experiment.

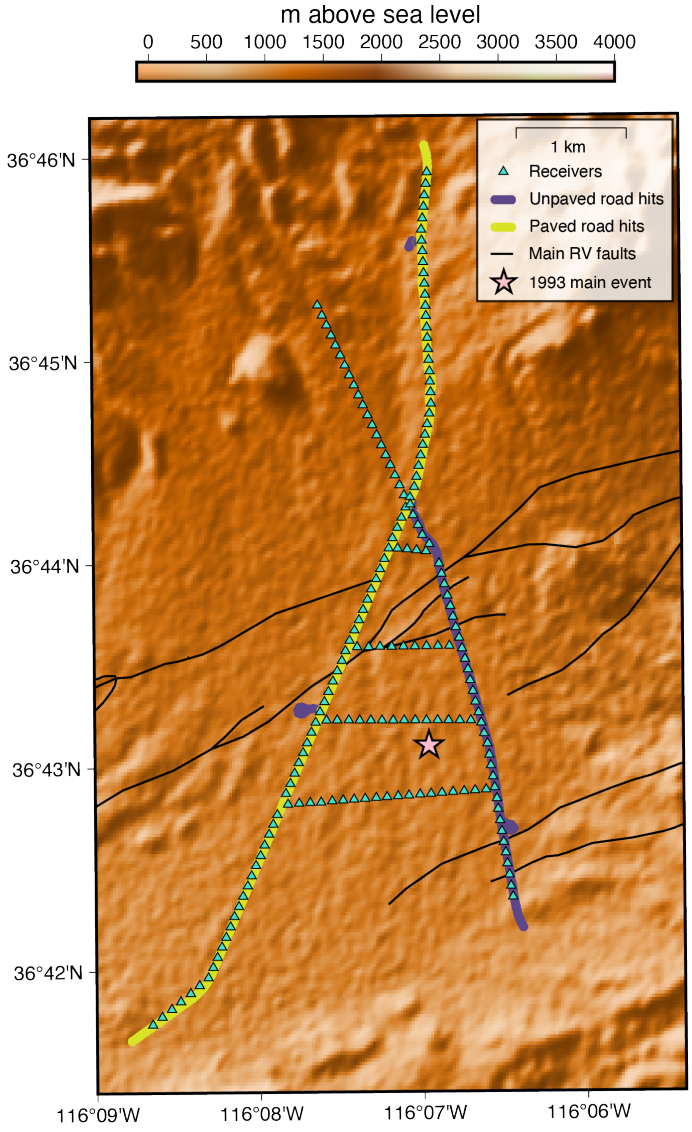

Figure 3-1. Study area and AWD experimental setup

Seismic signals were generated using an accelerated weight drop (AWD) source. The AWD can generate both P- and S-waves by driving a piston hammer into a metal foot both vertically and at a ~45° angle, respectively. The system mounts onto the rear-hitch of a pickup truck (Figure 3-2), is powered by a small diesel generator, and the piston is driven by compressed nitrogen. All the components are contained within the truck bed allowing for quick transit to each hit location. As such, all hit locations are limited by road access. For paved sections, sources were generated along the shoulder so as not to damage the road (yellow line in Fig. 3-1). The angle of the shoulder was often steep, which may affect the angle of the hit and, thus, whether a P- or S-wave is generated. For all shoulder cases we measured the angle of the foot and the AWD shaft for reference.

Figure 3-2. AWD system

We recorded hits every 25 m resulting in 553 source locations generated over 3 weeks in May and April 2021 (see Figure 3-1). The total length of the main lines was ~12.5 km, however, hits were also made on several short side roads for increased coverage. For each location we recorded at minimum 5 vertical hits (P), 5 horizontal hits – angled towards the driver side (S), and 5 horizontal hits – angled towards the passenger side (S). The truck was oriented generally south on the main lines to keep consistency between the horizontal hits. Where possible, the road was used to estimate the truck heading. On side roads we used survey instruments to estimate the heading. Each hit location was surveyed post-hit using high precision Global Positioning System (GPS) and the timing of the hits was recorded using a Seismic Signal Recorder (SeismicSource). Source data were monitored in real time and exact hit information was harvested after the experiment.

3.2. Waveform Processing

The AWD data, which include all three channel components for all vertical and horizontal hits, were cut and output into hit gathers in SEGY format. We attempted to cut the waveforms in accordance with the hit times with seismogram lengths of 9 s, so each seismogram began at the hit time to the nearest millisecond. There was, however, an error in how the VScope (SeismicSource) software output the hit times, so the waveform data were erroneously offset by

up to a second. We interpolated the seismograms to a sample rate of 1000 Hz in order to manually shift the time series to the milisecond using a separate file containing the hit times that was pulled directly from the Seismic Signal Recorder.

The hit gathers were read into MATLAB using a publicly-released toolbox from the Consortium for Research in Elastic Wave Exploration Seismology (CREWES) group at the University of Calgary, called the CREWES MATLAB Software Library (CMSL)(Margrave & Lamoureux, 2019). The data were wholly processed within MATLAB using the CMSL.

3.2.1. Vertical Hits

Within each hit gather, vertical hits on the Z channel were stacked, generally leading to a fold of 5. In order to stack, we had to first shift the seismograms to align the hit times at time zero. See Figure 3-3 for an example of a group of raw vertical hit seismograms, and their resultant stacked seismogram.

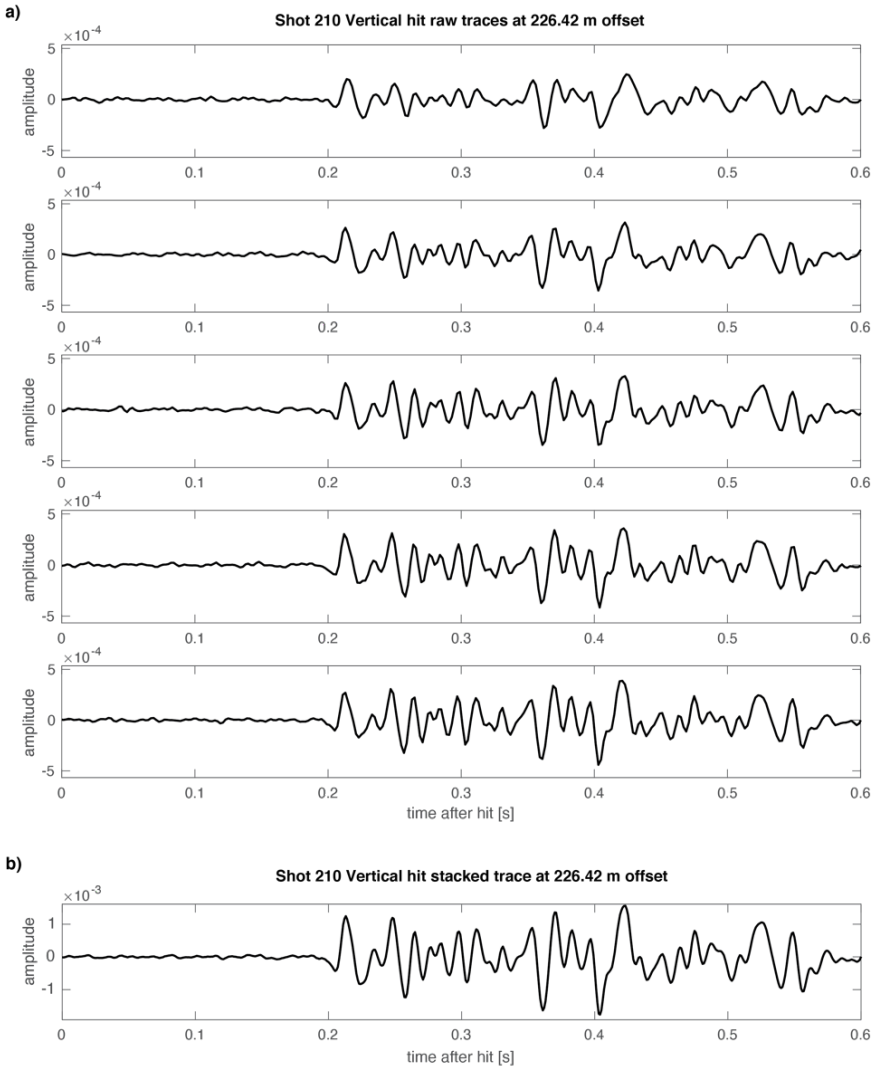

Figure 3-3. Raw vertical seismograms (a) and stacked seismogram example (b)

We then bandpass filtered the seismograms from 5 to 45 Hz using a Butterworth minimum-phase filter (Margrave & Lamoureux, 2019), which reduced noise for subsequent picking of P-wave and S-wave arrival times (Figure 3-4). The chosen filter maintains amplitudes well and improves the accuracy of arrival time picking, but potentially introduces a small (1-3 ms) bias to the picked travel-times. See Appendix B for further examples of filtered and unfiltered seismograms with picked arrival times. Seismograms were then sorted by source-receiver distance and normalized to produce the processed vertical hit gather. Figure 3-5 is an example of a processed vertical hit gather, where the first 60 shortest-offset seismograms are plotted as clipped (to 25%) variable area waveforms and offsets for specific seismograms are labeled along the top of the gather.

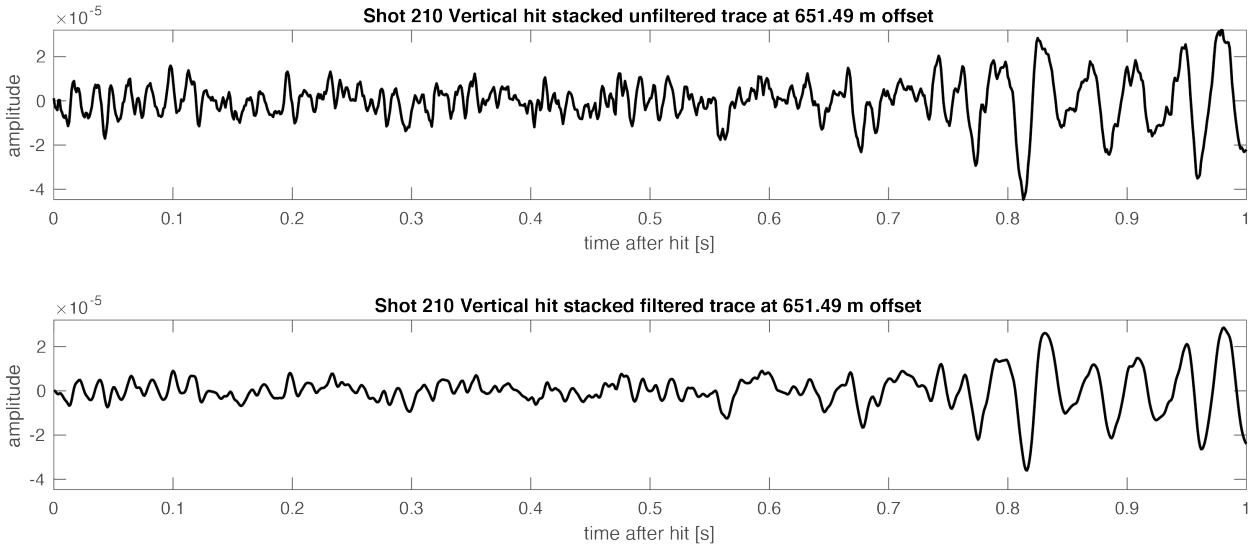

Figure 3-4. Vertical hit stacked seismogram, unfiltered vs. filtered

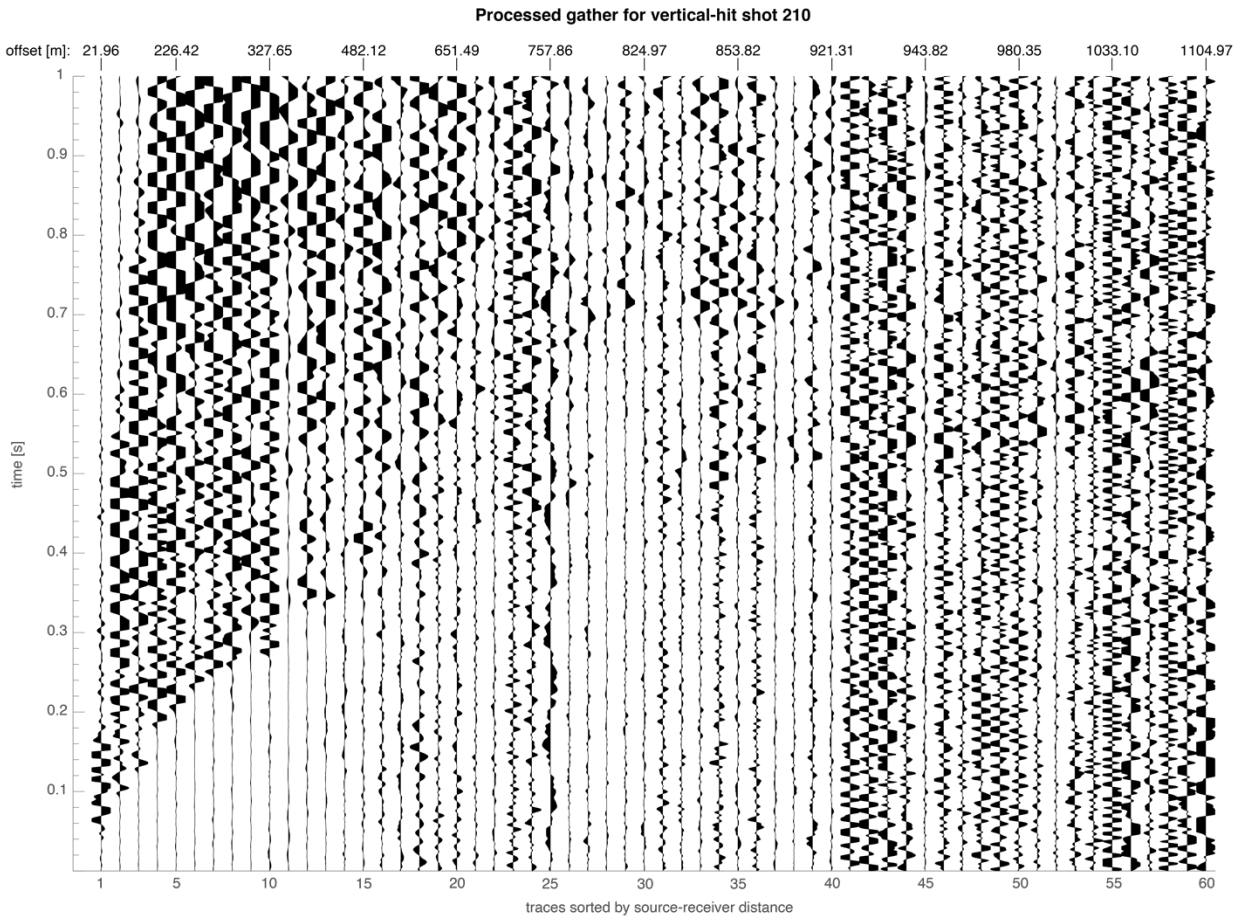

Figure 3-5. Processed vertical hit gather example

3.2.2. Horizontal Hits

Before processing the horizontal hit waveforms, we calculated the source-receiver back-azimuths, and only seismograms with back-azimuths within 0 ± 5° (and 180 ± 5°) of the truck heading, which is orthogonal to the horizontal hit directions (Figure 3-6), were included for processing. Theoretically, the transverse-component waveforms of the two horizontal hits at receivers with back-azimuths parallel to the truck heading will have in-phase P-waves and out-of-phase S-waves. Differencing the two horizontal hit waveforms, therefore, will result in a subdued P-wave arrival and an enhanced S-wave arrival.

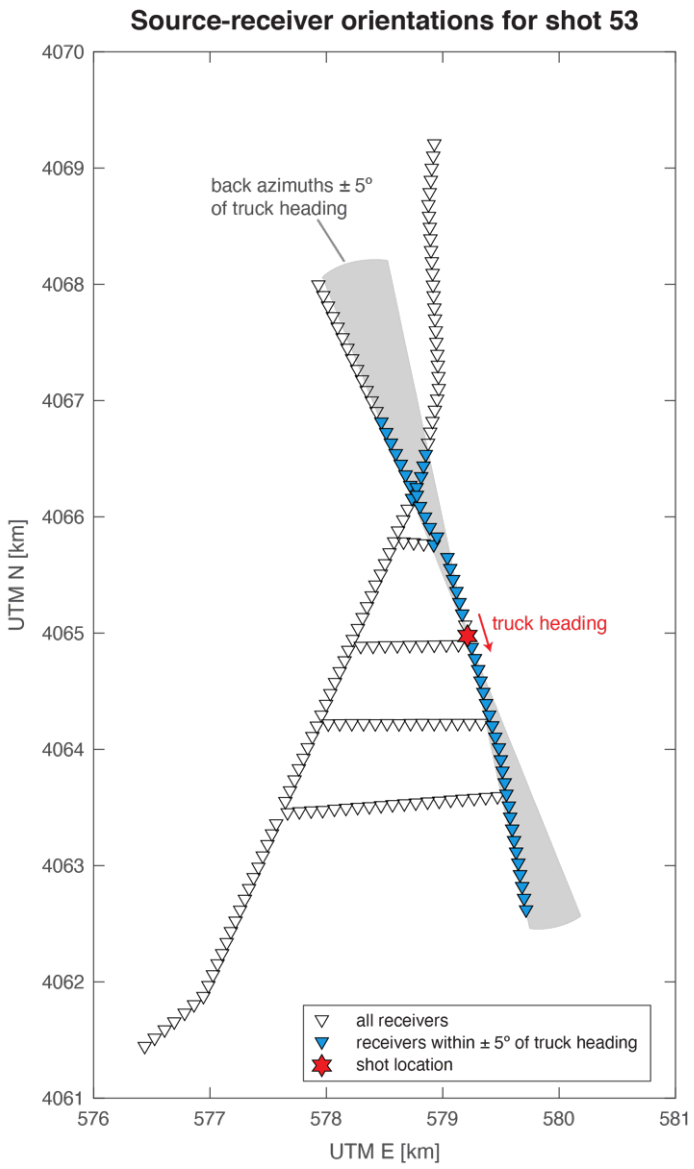

Figure 3-6. Source-receiver orientations example

We rotated the horizontal hit seismograms on North-South (NS) and East-West (EW) channels to obtain the transverse component, here meaning perpendicular to the truck heading and parallel to the horizontal hit directions for all receivers with back-azimuths ± 5° of the truck heading recorded in the field. As in the vertical hit processing, each horizontal hit seismogram was shifted so the hit occurs at time zero, then stacked for an average fold of 5. See Figure 3-7 and Figure 3-8 for examples of raw horizontal hits +90° and -90° from the truck heading on NS and EW channels, respectively.

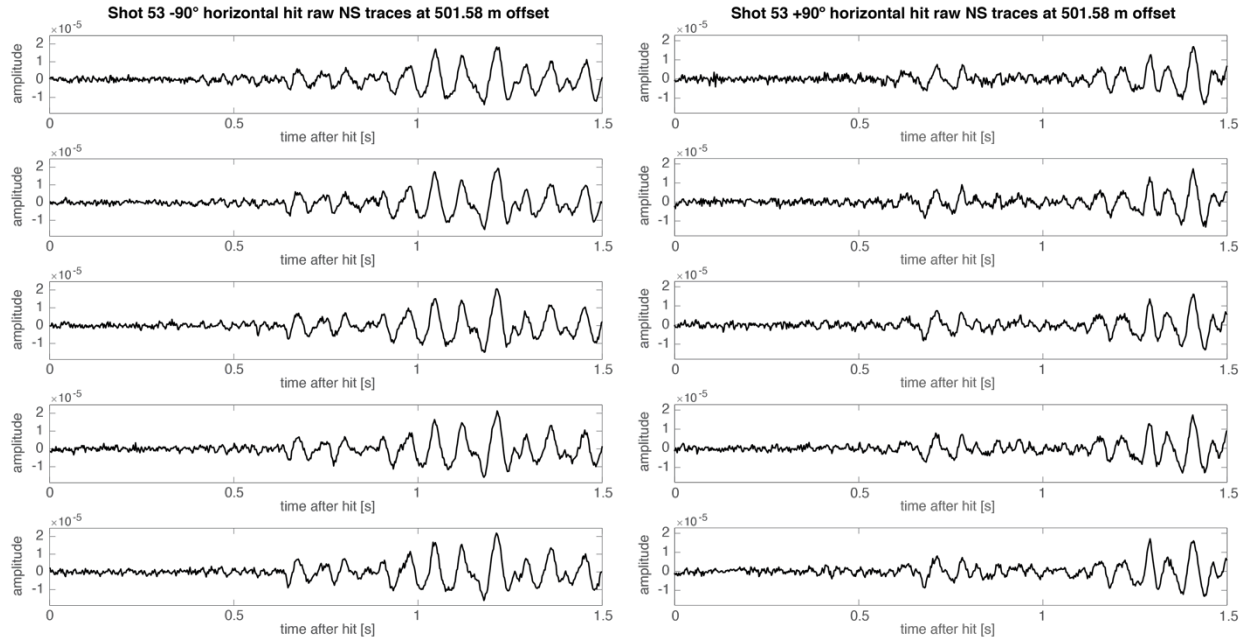

Figure 3-7. Raw NS horizontal hit seismograms example

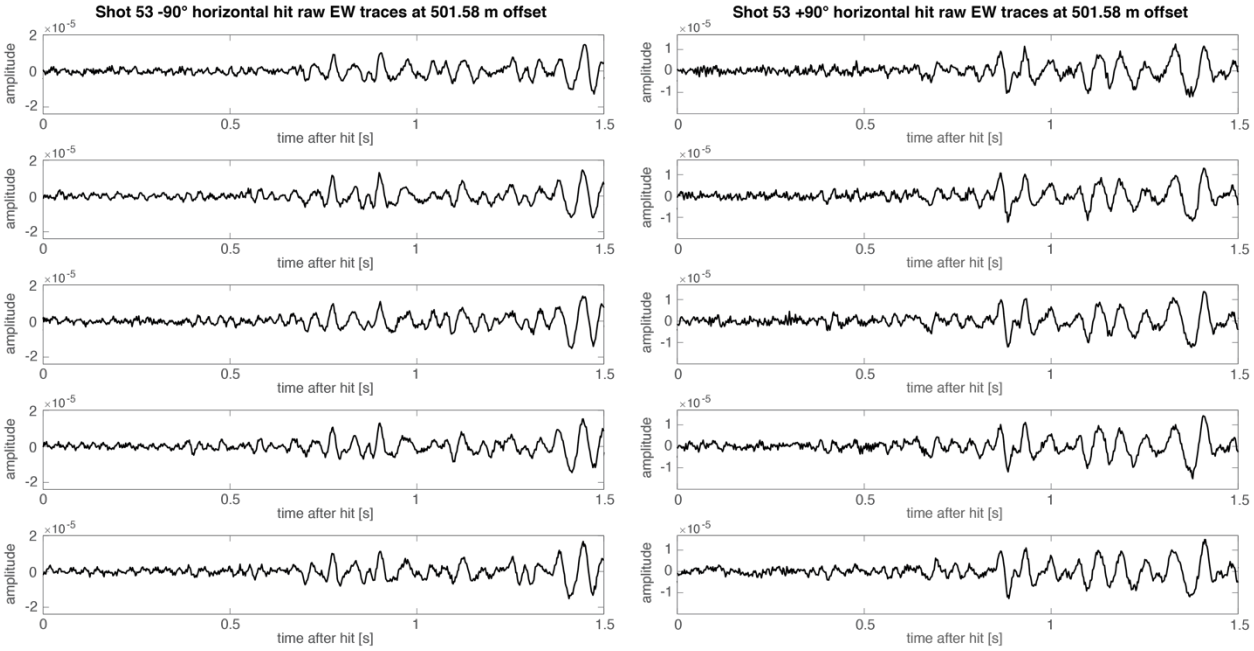

Figure 3-8. Raw EW horizontal hit seismograms example

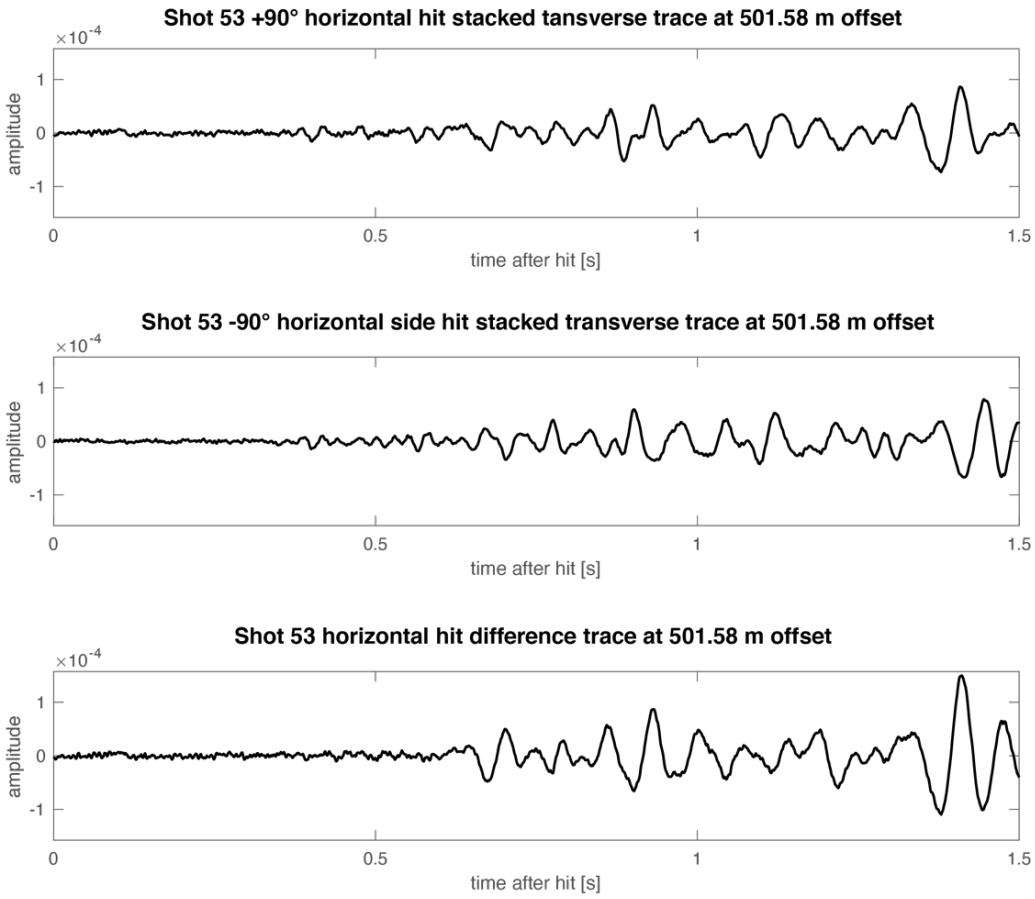

Figure 3-9. Horizontal hit stacks and horizontal hit difference stack example

The two horizontal hit stacks were then differenced to reduce the P-wave arrival and enhance the S-wave arrival. Figure 3-9 shows an example of a left and right horizontal hit transverse-component stacked seismogram, and the difference between the two seismograms. We filtered the stacked horizontal hit difference seismograms using a Butterworth, minimum-phase, bandpass filter from 5-45 Hz to reduce noise and improve the accuracy of S-wave arrival-time picking (Figure 3-10, Appendix B). See Figure 3-11 for an example of a processed horizontal hit difference gather, where seismograms are sorted by offset, normalized, and plotted as clipped (to 60%) variable waveforms. Seismograms from receivers with back-azimuths >5° from the truck heading are not included in the gather plot. As in the vertical hit processed gathers, seismograms in the processed horizontal hit difference gathers are sorted by source-receiver distance, and offsets for specific seismograms are labeled along the top of the gather.

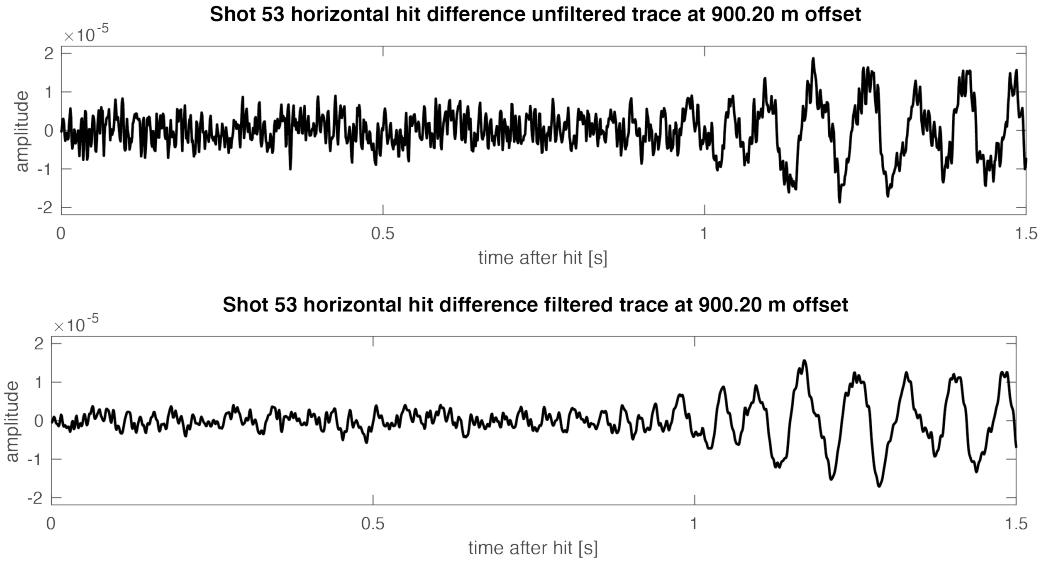

Figure 3-10. Horizontal hit difference stacked seismogram, filtered vs. unfiltered

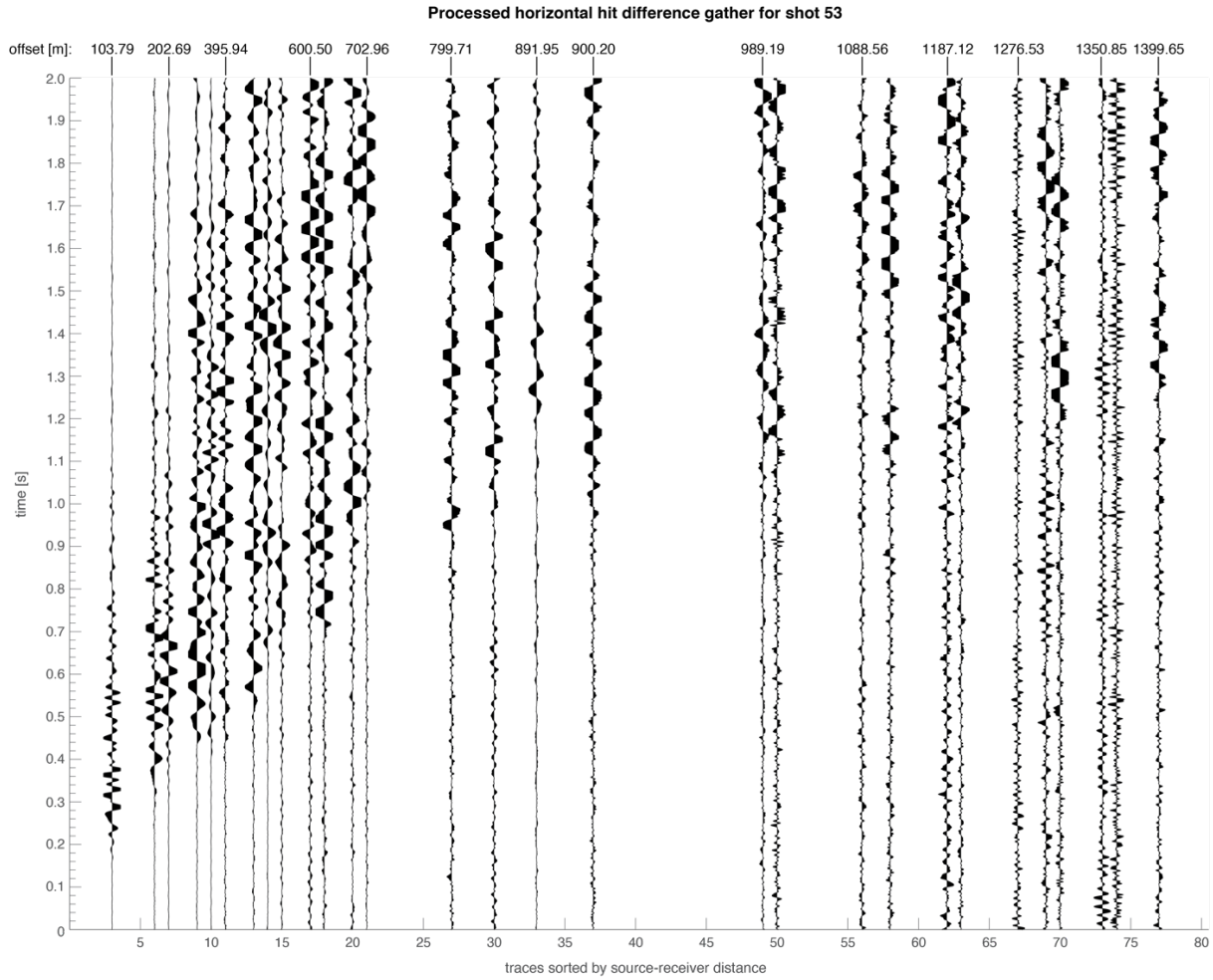

Figure 3-11. Processed horizontal hit difference gather

3.3. Picking P-wave and S-wave arrival times

3.3.1. P-wave Arrival Time Picks

P-waves arrival times were picked on processed vertical hit gathers. In total, 7,982 P-wave arrivals were picked on 550 out of 553 hit gathers. The median number of P-wave arrival picks per gather is 13 and the median maximum offset picked on gathers is ~689 m. Figure 3-12 summarizes the P-wave arrival pick statistics.

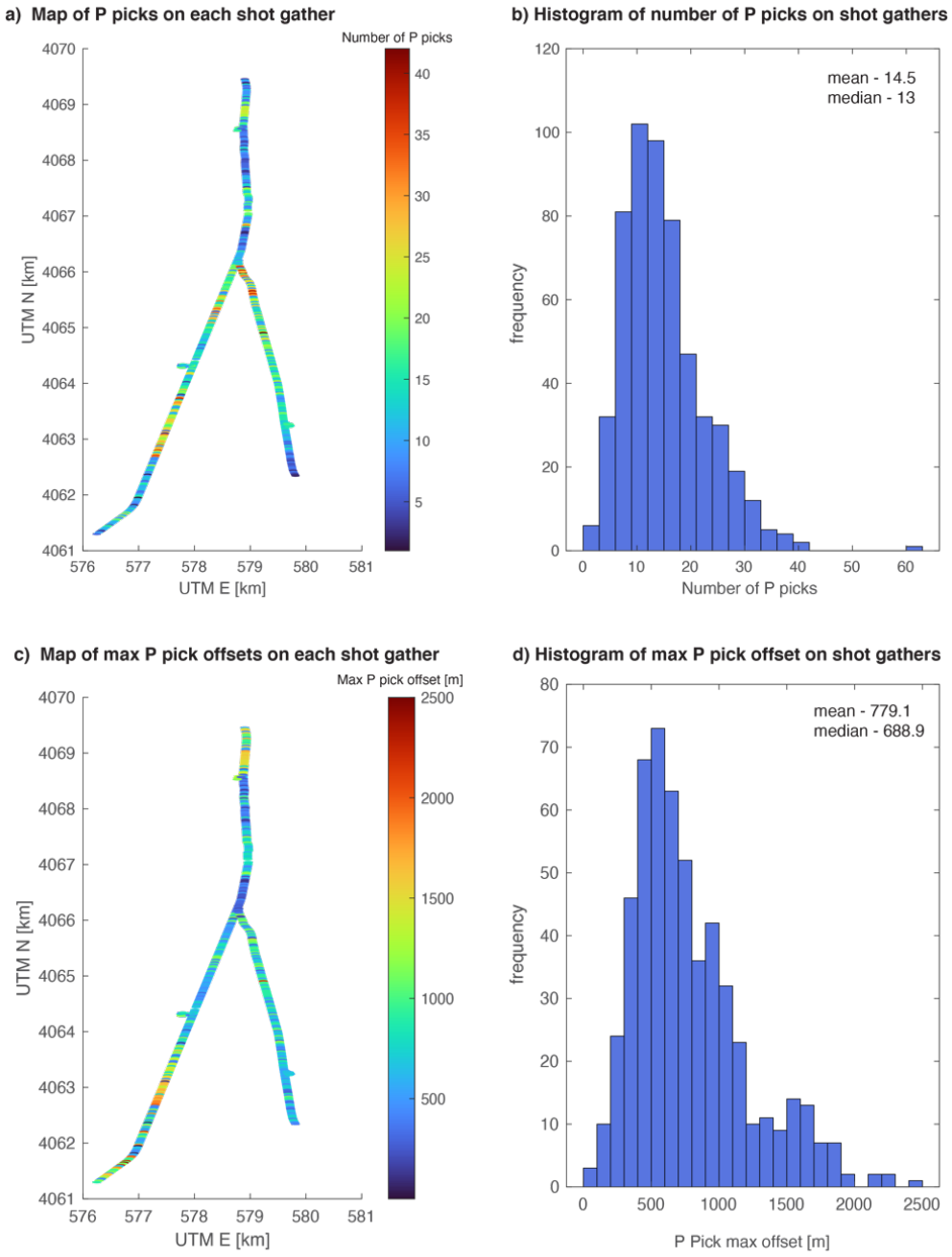

Figure 3-12. Summary of P-wave picked arrival times

Error codes were assigned to P-wave arrival time picks during the picking process, and error times were later assigned to those codes. Error codes range from 1 to 4, where 1 indicates a good pick with minimal noise and 4 indicates a poor picked arrival time with low signal-to-noise. Table 3-1. P-wave arrival time pick error assignments explains the error codes and associated error in milliseconds and Figure 3-13 shows a histogram of the P-wave picked arrival time error codes. In addition to error times, binary confidences were assigned to all picks, where 1 indicates the pick very likely sits within the assigned error bounds, and 0 indicates that the P arrival was uncertain and the true arrival could fall outside the assigned error bounds. See Figure 3-14 and Figure 3-15 for examples of P-wave arrival time picks on two processed gathers.

Table 3-1. P-wave arrival time pick error assignments

Error Code	Assigned Error	Description
1	± 2 ms	Very good pick, little to no noise at P arrival
2	± 10 ms	Good pick, little noise at P arrival
3	± 20 ms	Fair pick, some noise at P arrival
4	± 40 ms	Poor pick, noise at P arrival

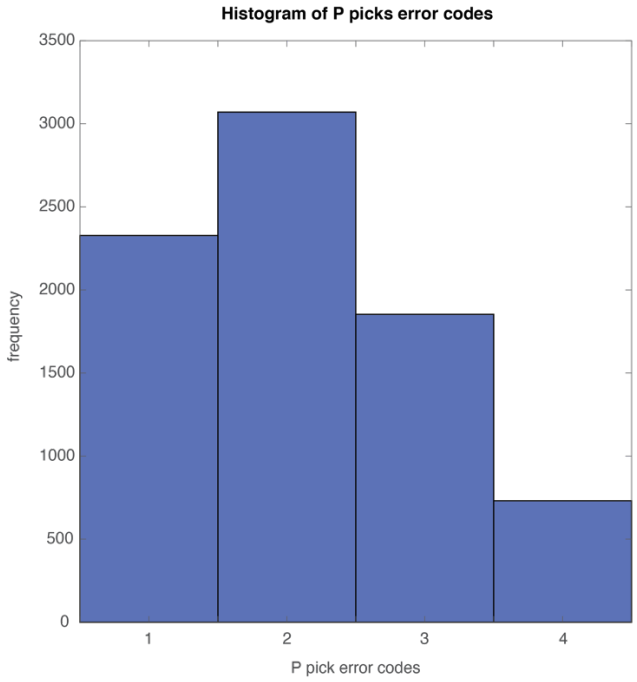

Figure 3-13. P-wave arrival time pick error code histogram

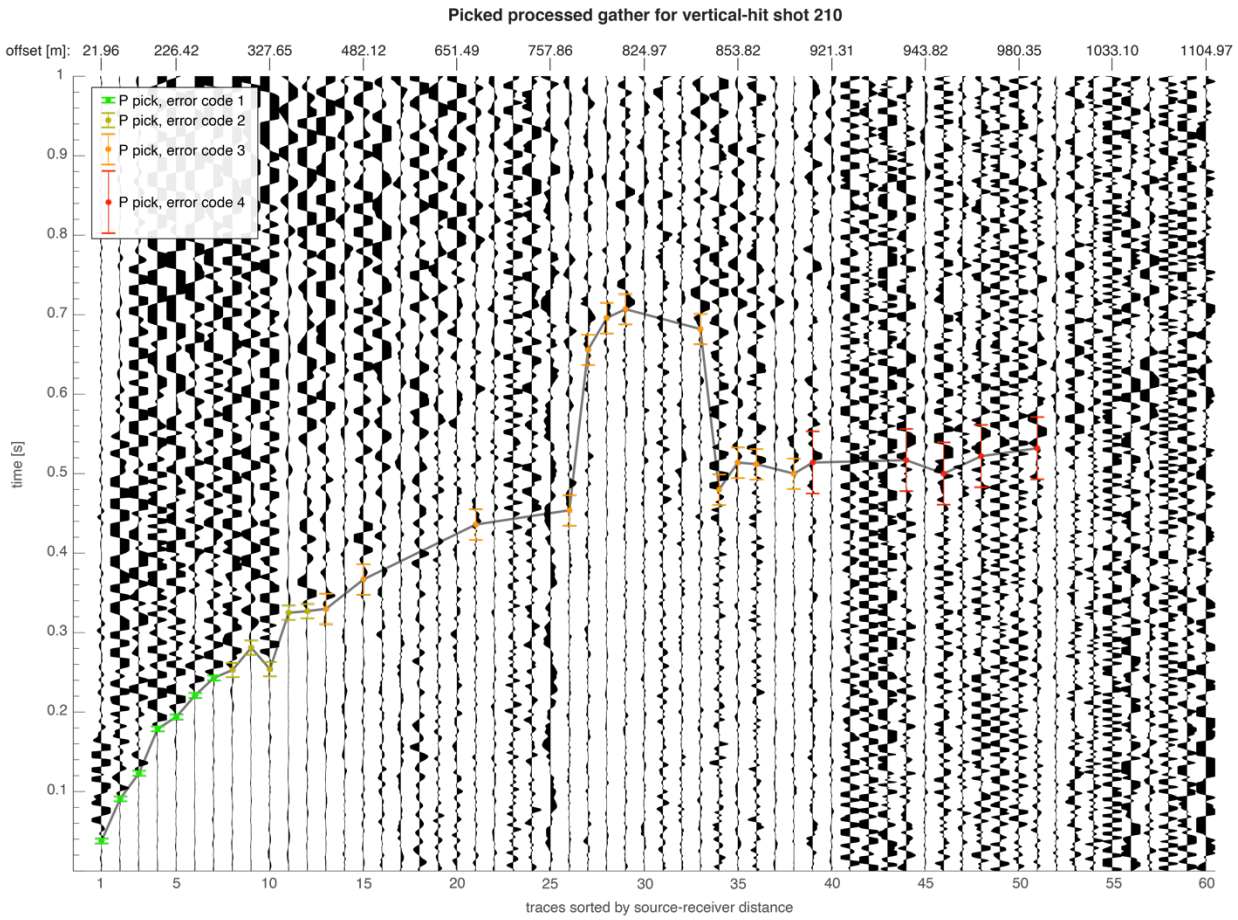

Figure 3-14. P-wave arrival time picks shown on processed vertical hit gather 210

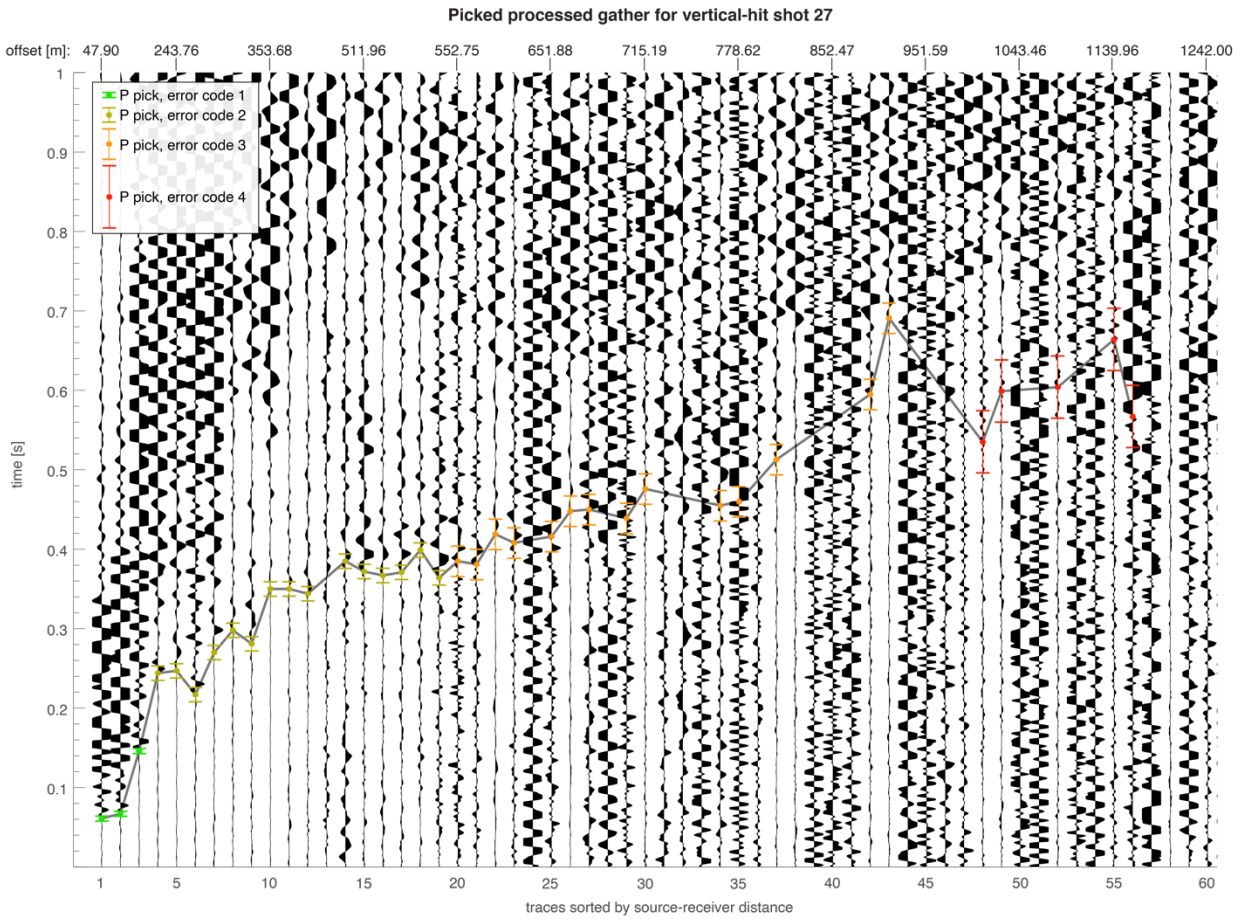

Figure 3-15. P-wave arrival time picks shown on processed vertical hit gather 27

3.3.2. S-wave Arrival Time Picks

S-wave arrival times were picked on processed horizontal hit difference gathers. There were 4,369 S-waves arrivals times picked in total on 465 out of 553 of the hit gathers. The median number of S-wave arrival time picks made on gathers is 8, and the median maximum offset picked on hit gathers is 778 m. Figure 3-16 shows maps and histograms of the S-wave arrival pick statistics.

As in the P-wave picking process, error codes 1-4 were assigned to S-wave arrival time picks. The error times and descriptions are in Table 3-2, and a histogram of the assigned error codes is in Figure 3-17. Binary confidences were also assigned, where 0 indicates that the S arrival might fall outside of the assigned error, and 1 indicates that the pick confidently falls within the error bounds. Examples of S-wave arrival time picks on processed horizontal hit difference gathers can be seen in Figure 3-18 and Figure 3-19, where pick colors show the assigned error codes.

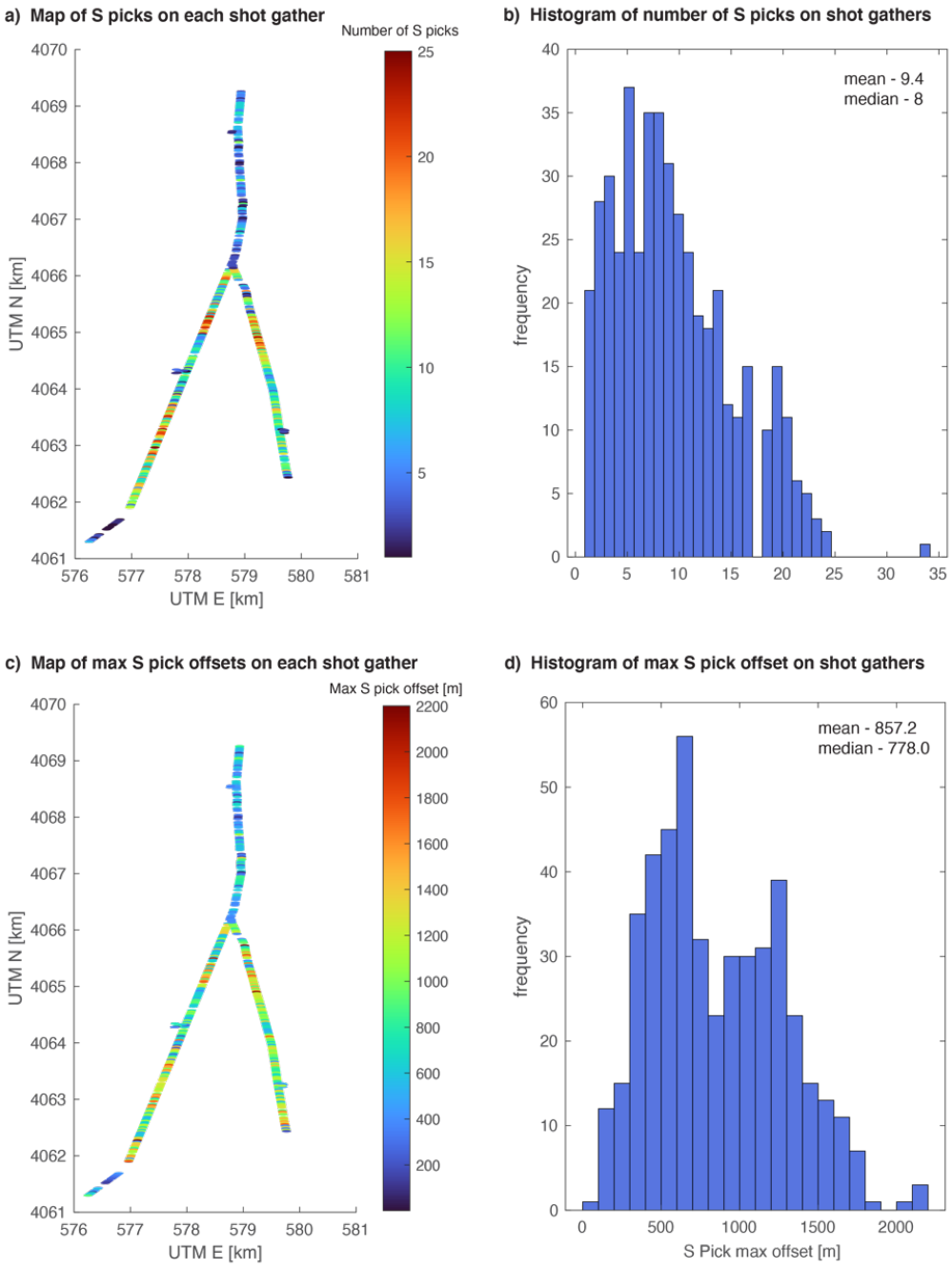

Figure 3-16. Summary of S-wave arrival time picks

Table 3-2. S-wave arrival time pick error assignments

Error Code	Assigned Error	Description
1	± 10 ms	Very good pick, little to no noise at S arrival
2	± 20 ms	Good pick, little noise at S arrival
3	± 40 ms	Fair pick, some noise at S arrival
4	± 80 ms	Poor pick, noise at S arrival

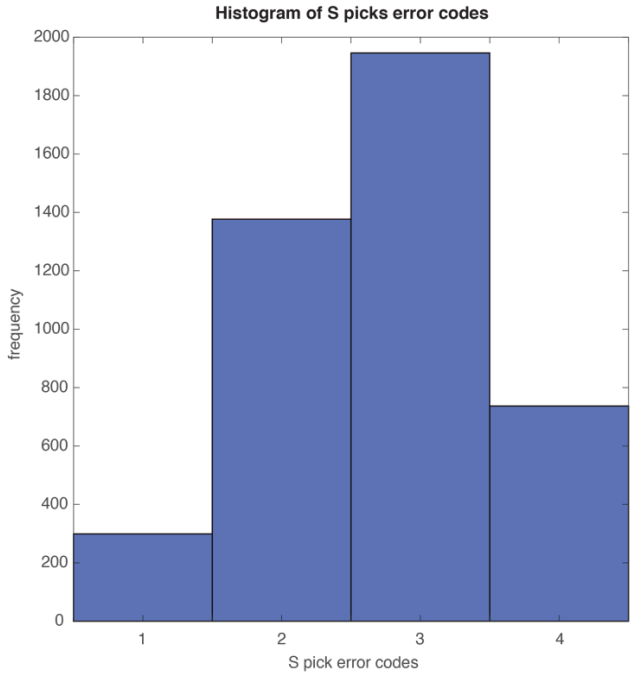

Figure 3-17. S-wave arrival time pick error code histogram

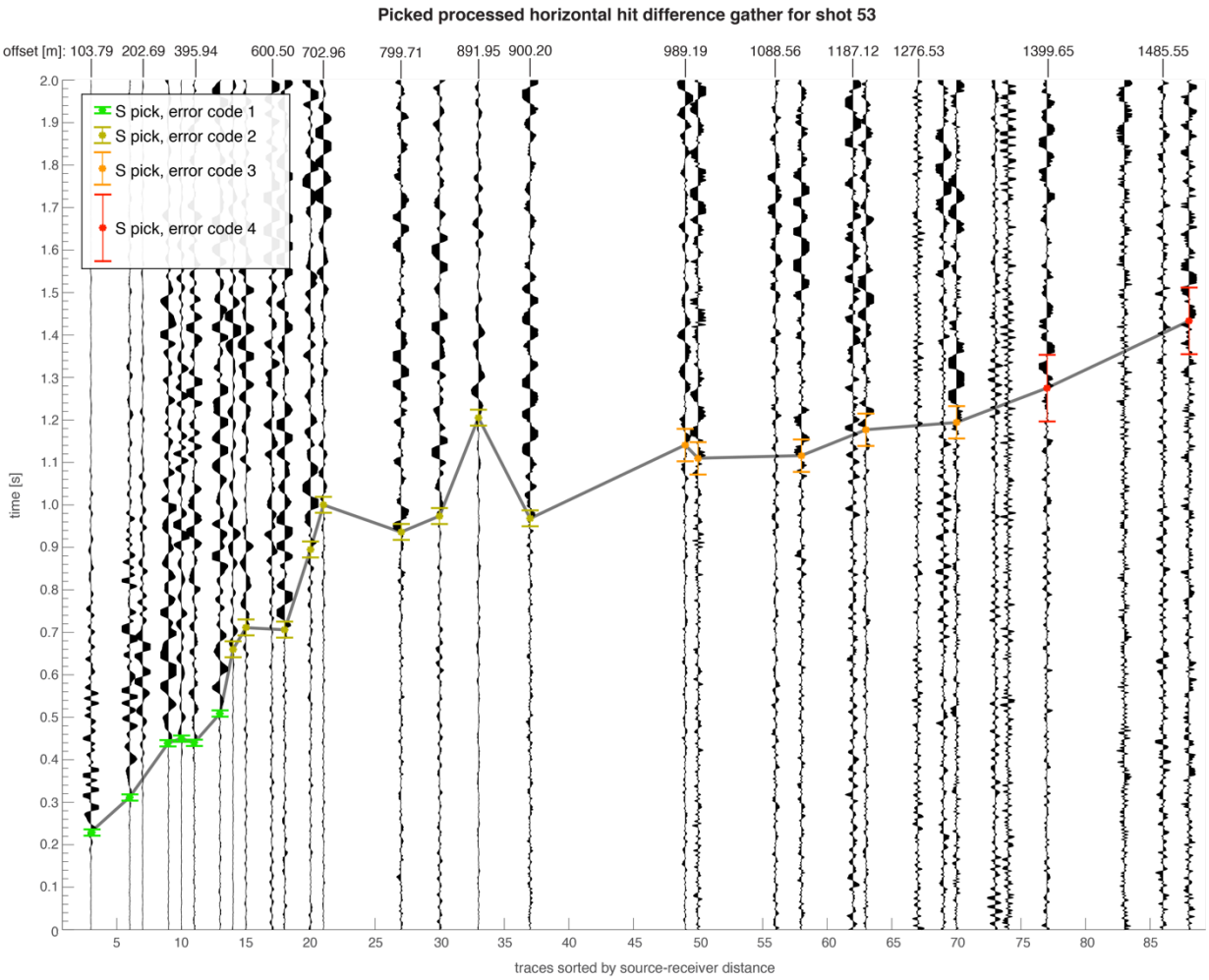

Figure 3-18. S-wave arrival time picks shown on processed horizontal hit difference gather 53

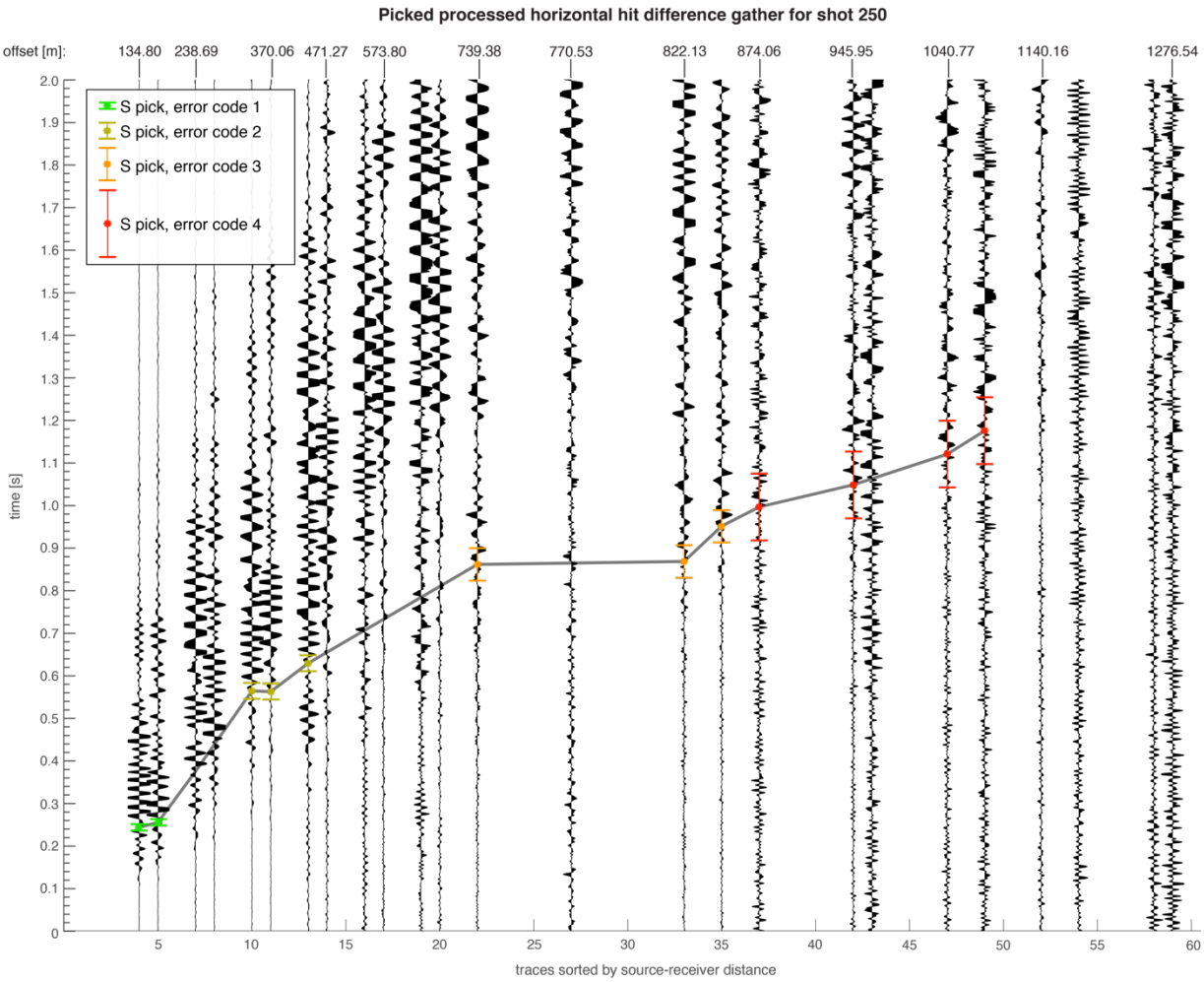

Figure 3-19. S-wave arrival time picks shown on processed horizontal hit difference gather 250

This page left blank

4. SUMMARY

AWD data were collected in April and May of 2021 in Rock Valley, around the region where a shallow cluster of earthquakes occurred in 1993. We processed the waveforms to vertical hit gathers and horizontal hit difference gathers, which we then picked for P-wave and S-wave travel-times. In total, 7,982 P picks and 4,369 S picks were made. This dataset can be used in future studies to image the shallow P-wave and S-wave velocities in the region, and a preliminary P-wave velocity model is presented in Preston & Harding (2021).

REFERENCES

Barnes, H., Ekren, E. B., Rodgers, C. L., & Hedlund, D. C. (1982). Geologic and tectonic maps of the Mercury quadrangle, Nye and Clark Counties, Nevada (No. 1197).

O'Leary, D. W., Whitney, J. W., & Keefer, W. R. (2000). Tectonic significance of the Rock Valley fault zone, Nevada Test Site. Geologic and Geophysical Characterization Studies of Yucca Mountain, Nevada, A Potential High-Level Radioactive-Waste Repository, edited by JW Whitney and WR Keefer, Digital Data Ser, 58.

JPL, N. (2013). NASA Shuttle Radar Topography Mission Global 1 arc second. Version 3. NASA EOSDIS LP DAAC; USGS Earth Resources Observation and Science (EROS) Center: Sioux Falls, SD, USA.

Kane, M. F., & Bracken, R. E. (1983). Aeromagnetic map of Yucca Mountain and surrounding regions, southwest Nevada(No. USGS-OFR--83-616). Geological Survey.

Majer, E., Feighner, M., Johnson, L., Daley, T., Karageorgi, E., Lee, K. H., ... & McEvilly, T. (1996). Synthesis of borehole and surface geophysical studies at Yucca Mountain. Nevada and vicinity, 1.

Margrave, G. F., & Lamoureux, M. P. (2019). Numerical methods of exploration seismology: With algorithms in MATLAB®. Cambridge University Press.

Preston, L., Harding, J.L. (2021). Rock Valley Accelerated Weight Drop Preliminary P-wave Tomographic Model. SAND2021-XXXX, Sandia National Laboratories, Albuquerque, NM

Preston, L., Smith, K., & von Seggern, D. (2007). P wave velocity structure in the Yucca Mountain, Nevada, region. Journal of Geophysical Research: Solid Earth, 112(B11).

Preston, L., Poppeliers, C., & Schodt, D. J. (2019). Seismic Characterization of the Nevada National Security Site Using Joint Body Wave, Surface Wave, and Gravity Inversion. Bulletin of the Seismological Society of America, 110(1), 110-126.

Pyle, M. L., Myers, S. C., Walter, W. R., & Smith, K. D. (2015). Accurate local event locations in Rock Valley, Nevada, using a Bayesian multiple-event method. Bulletin of the Seismological Society of America, 105(2A), 706-718.

Sinnock, S. (1982). Geology of the Nevada Test Site and nearby areas, southern Nevada. Sandia National Laboratories.

Slate, J. L., Berry, M. E., Rowley, P. D., Fridrich, C. J., Morgan, K. S., Workman, J. B., ... & Jayko, A. S. (1999). Digital geologic map of the Nevada Test Site and vicinity, Nye, Lincoln, and Clark Counties, Nevada, and Inyo County, California (No. USGS/OFR-99-554). Geological Survey, Las Vegas, NV (US).

Smith, K. D., Brune, J. N., & Shields, G. (2000). A sequence of very shallow earthquakes in the Rock Valley fault zone, southern Nevada Test Site. EOS suppl, 74, 417.

Yount, J. C., Shroba, R. R., McMasters, C. R., Huckins, H. E., & Rodriguez, E. A. (1987). Trench logs from a strand of the Rock Valley fault system, Nevada Test Site, Nye County, Nevada (No. USGS/MAP/MF-1824). Geological Survey, Reston, VA (United States).

APPENDIX A. CORRELATION OF NNSS GEOLOGIC MAP UNITS

A complete description of the geologic units of the RV area can be found in Slate et al. (1999). Figure A-1 (from Slate et al., 1999) provides a summary of the geologic units in Figure 2-1c.

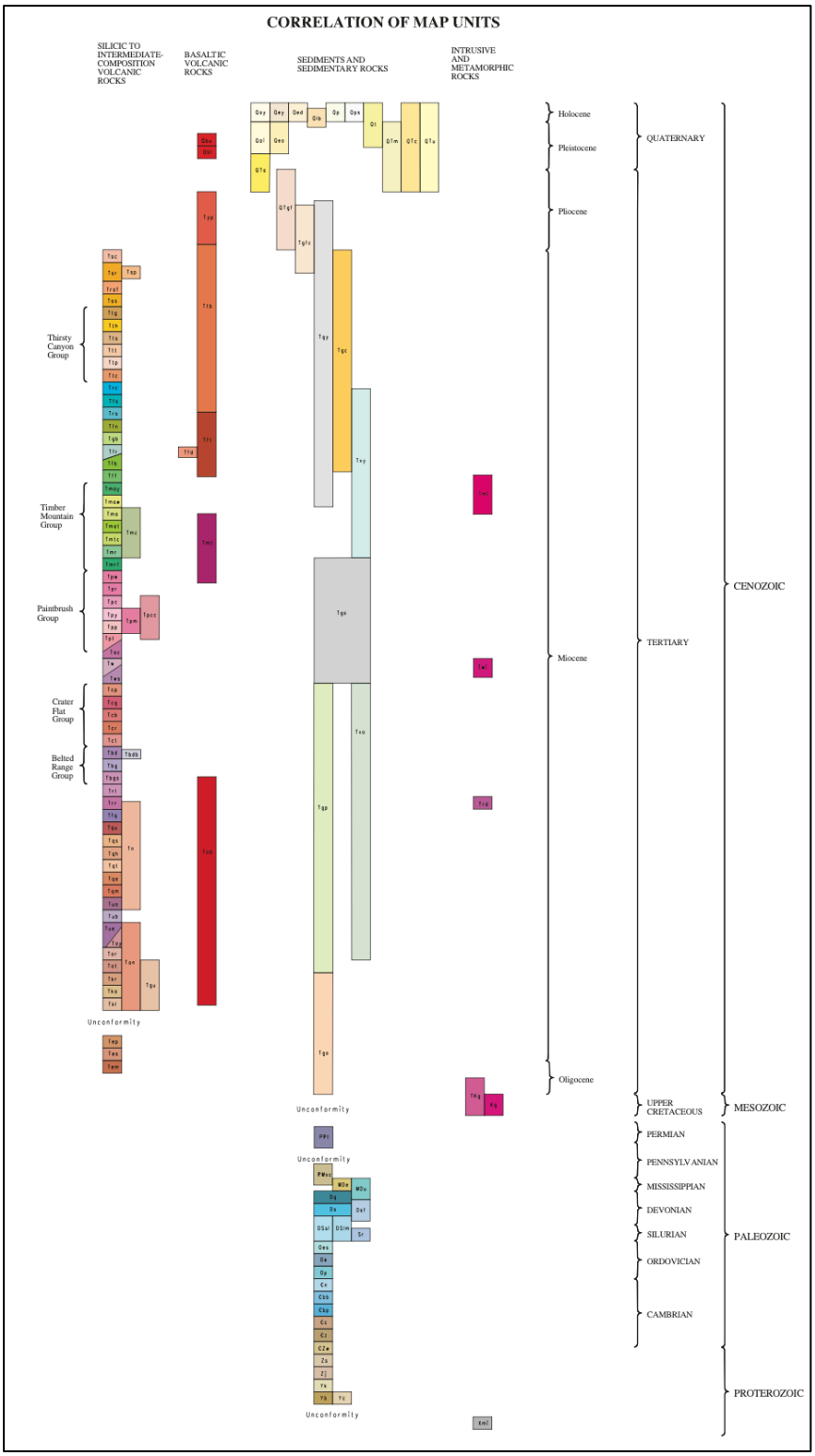

Figure A-1. Correlation of Geologic Units in Figure 2-1c

APPENDIX B. SEISMOGRAM FILTERING

All stacked seismograms were filtered using a causal, minimum-phase Butterworth bandpass filter (Margrave & Lamoureux, 2019). Filtering the waveform data improved the signal-to-noise ratio, which led to more accurate arrival picking, as well as expanded the number of seismograms that could be picked for P-wave and S-wave arrival times. We chose a minimum-phase filter over a zero-phase filter for its causality, as well as its ability to better maintain amplitudes (Figure B-1).

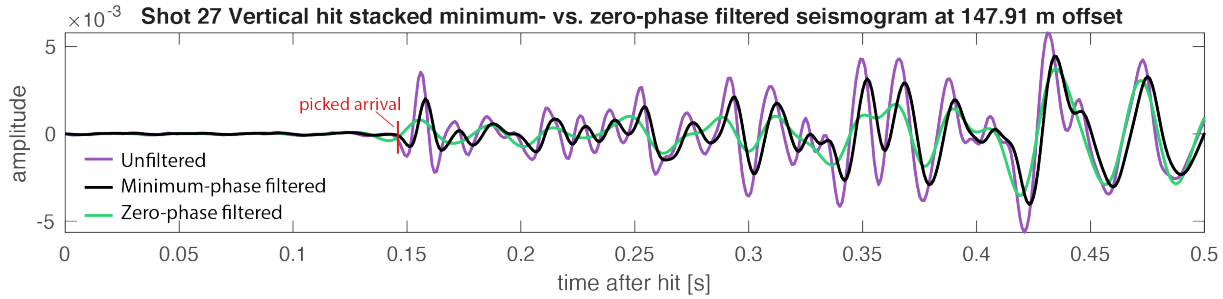

Figure B-1. Example of minimum-phase vs. Zero-phase filtering of stacked vertical hit seismogram

Additionally, at near-offset seismograms, the zero-phase filter had the tendency to shift the first arrival P-wave earlier on the order of 0.01 s (Figure B-1). Our chosen minimum-phase filter, however, has the potential to bias the picking of P-wave and S-wave arrival times later by 1-3 ms. See Figure B-2 and Figure B-3 for examples of filtered and infiltered processed seismograms with the picked arrival time for P-wave and S-waves, respectively.

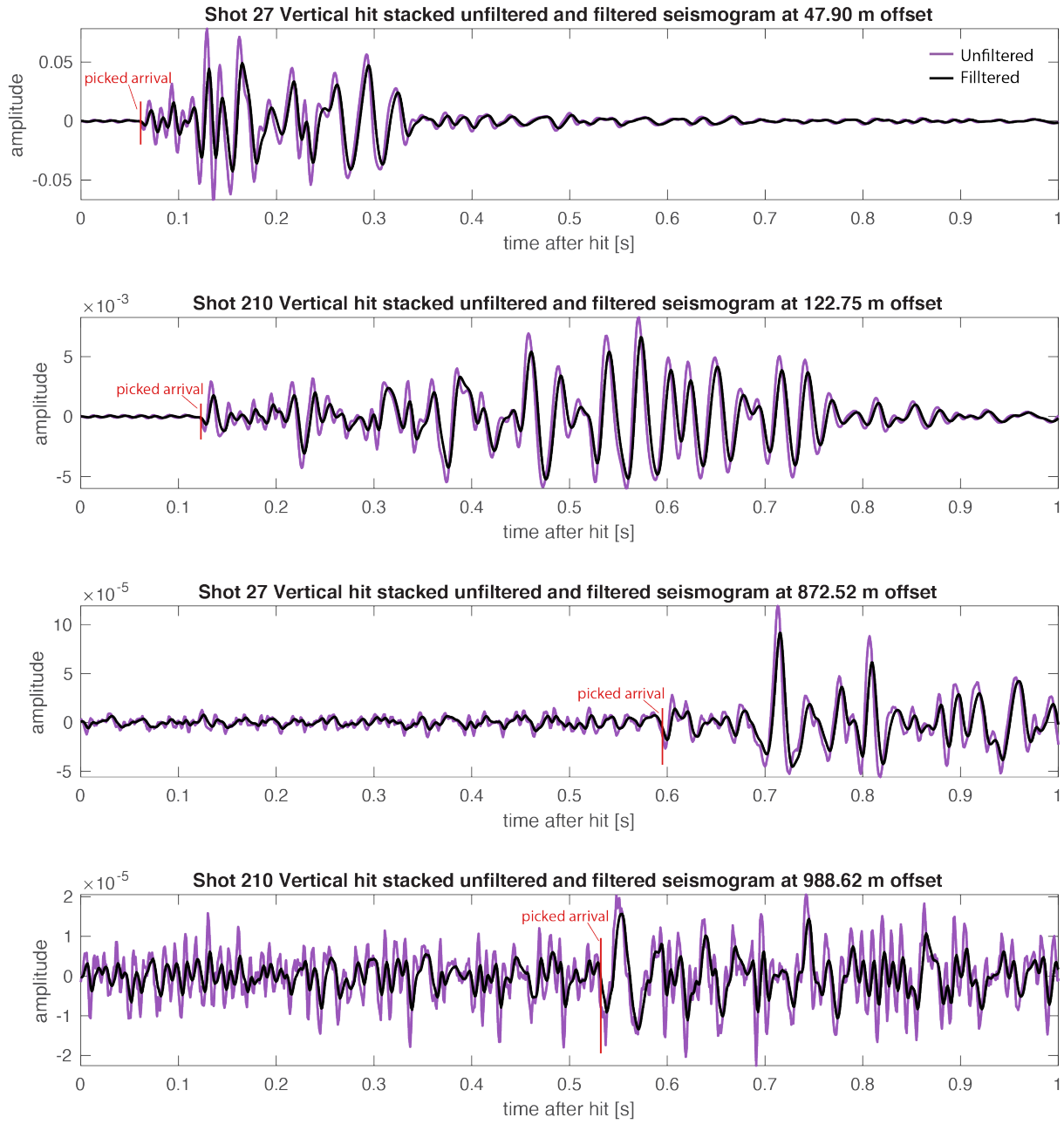

Figure B-2. Examples of filtered and unfiltered stacked vertical hit seismograms

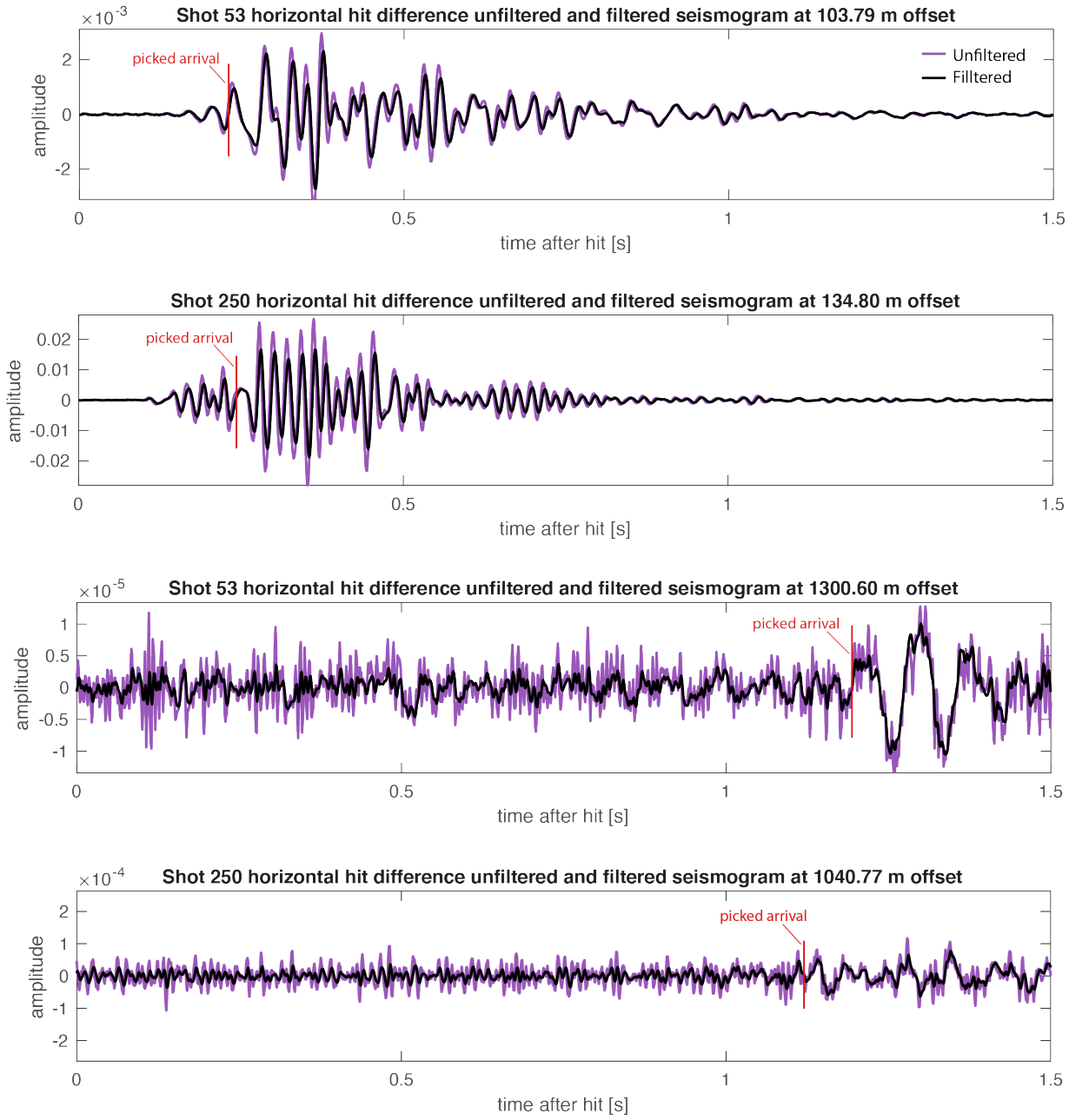

Figure B-3. Examples of filtered and unfiltered horizontal hit difference seismograms

DISTRIBUTION

Email—Internal

Name	Org.	Sandia Email Address
Rob Abbott	8911	reabbot@sandia.gov
Christian Poppeliers	8911	cpoppel@ssandia.gov
Technical Library	01977	sanddocs@sandia.gov

This page left blank

This page left blank

Sandia National Laboratories

Sandia National Laboratories is a multimission laboratory managed and operated by National Technology & Engineering Solutions of Sandia LLC, a wholly owned subsidiary of Honeywell International Inc. for the U.S. Department of Energy's National Nuclear Security Administration under contract DE-NA0003525.